

## New insight into the Rapid Burster by Insight-HXMT

Y. P. CHEN<sup>\*</sup>,<sup>1</sup> S. ZHANG<sup>\*</sup>,<sup>1</sup> S. N. ZHANG,<sup>1,2</sup> L. JI,<sup>3</sup> L. D. KONG,<sup>1,2</sup> P. J. WANG,<sup>1,2</sup> L. TAO,<sup>1</sup> M. Y. GE,<sup>1</sup> C. Z. LIU,<sup>1</sup> F. J. LU,<sup>1</sup> J. L. QU,<sup>1,2</sup> T. P. LI,<sup>1,4,2</sup> Y. P. XU,<sup>1</sup> X. L. CAO,<sup>1</sup> Y. CHEN,<sup>1</sup> Q. C. BU,<sup>1</sup> C. CAI,<sup>1</sup> Z. CHANG,<sup>1</sup> G. CHEN,<sup>1</sup> L. CHEN,<sup>5</sup> T. X. CHEN,<sup>1</sup> W. W. CUI,<sup>1</sup> Y. Y. DU,<sup>1</sup> G. H. GAO,<sup>1,2</sup> H. GAO,<sup>1,2</sup> M. GAO,<sup>1</sup> Y. D. GU,<sup>1</sup> J. GUAN,<sup>1</sup> C. C. GUO,<sup>1,2</sup> D. W. HAN,<sup>1</sup> Y. HUANG,<sup>1</sup> J. HUO,<sup>1</sup> S. M. JIA,<sup>1</sup> W. C. JIANG,<sup>1</sup> J. JIN,<sup>1</sup> B. LI,<sup>1</sup> C. K. LI,<sup>1</sup> G. LI,<sup>1</sup> W. LI,<sup>1</sup> X. LI,<sup>1</sup> X. B. LI,<sup>1</sup> X. F. LI,<sup>1</sup> Z. W. LI,<sup>1</sup> X. H. LIANG,<sup>1</sup> J. Y. LIAO,<sup>1</sup> B. S. LIU,<sup>4</sup> H. W. LIU,<sup>1</sup> H. X. LIU,<sup>1</sup> X. J. LIU,<sup>1</sup> X. F. LU,<sup>1</sup> Q. LUO,<sup>1,2</sup> T. LUO,<sup>1</sup> R. C. MA,<sup>1</sup> X. MA,<sup>1</sup> B. MENG,<sup>1</sup> Y. NANG,<sup>1,2</sup> J. Y. NIE,<sup>1</sup> G. OU,<sup>1</sup> N. SAI,<sup>1,2</sup> L. M. SONG,<sup>1,2</sup> X. Y. SONG,<sup>1</sup> L. SUN,<sup>1</sup> Y. TAN,<sup>1</sup> Y. L. TUO,<sup>1,2</sup> C. WANG,<sup>6,2</sup> L. J. WANG,<sup>5</sup> W. S. WANG,<sup>1</sup> Y. S. WANG,<sup>1</sup> X. Y. WEN,<sup>1</sup> B. B. WU,<sup>1</sup> B. Y. WU,<sup>1,2</sup> M. WU,<sup>1</sup> G. C. XIAO,<sup>1,2</sup> S. XIAO,<sup>1,2</sup> S. L. XIONG,<sup>1</sup> R. J. YANG,<sup>7</sup> S. YANG,<sup>1</sup> Y. J. YANG,<sup>1</sup> Y. J. YANG,<sup>1</sup> Q. B. YI,<sup>1,2</sup> Q. Q. YIN,<sup>1</sup> Y. YOU,<sup>1</sup> F. ZHANG,<sup>1</sup> H. M. ZHANG,<sup>1</sup> J. ZHANG,<sup>1</sup> W. C. ZHANG,<sup>1</sup> W. ZHANG,<sup>1,2</sup> Y. ZHANG,<sup>1</sup> Y. F. ZHANG,<sup>1</sup> Y. H. ZHANG,<sup>1,2</sup> H. S. ZHAO,<sup>1</sup> X. F. ZHAO,<sup>1,2</sup> S. J. ZHENG,<sup>1</sup> Y. G. ZHENG,<sup>1,7</sup> AND D. K. ZHOU<sup>1,2</sup>

<sup>1</sup>Key Laboratory for Particle Astrophysics, Institute of High Energy Physics, Chinese Academy of Sciences, 19B Yuquan Road, Beijing 100049, China

<sup>2</sup>University of Chinese Academy of Sciences, Chinese Academy of Sciences, Beijing 100049, China

<sup>3</sup>Institut für Astronomie und Astrophysik, Kepler Center for Astro and Particle Physics, Eberhard Karls, Universität, Sand 1, D-72076 Tübingen, Germany

<sup>4</sup>Department of Astronomy, Tsinghua University, Beijing 100084, China

<sup>5</sup>Department of Astronomy, Beijing Normal University, Beijing 100088, China

<sup>6</sup>Key Laboratory of Space Astronomy and Technology, National Astronomical Observatories, Chinese Academy of Sciences, Beijing 100012, China

<sup>7</sup>College of physics Sciences & Technology, Hebei University, No. 180 Wusi Dong Road, Lian Chi District, Baoding City, Hebei Province 071002, China

Submitted to ApJ

### ABSTRACT

We report the timing and spectral analyses upon of the type II X-ray bursts from the Rapid Burster (MXB 1730–335) observed by Insight-HXMT and Swift/XRT. **By stacking the long-duration bursts, we find for the first time that the hard X-rays are lagging than the soft X-rays by 3 seconds. However, such a lag is not visible for the short-duration bursts, probably because of the poor statistics. For all bursts the energy spectrum is found to be non-thermal, thanks to the broad band coverage of Insight-HXMT. These findings put new insights into the type-II bursts and require a temporally showing-up corona for possible interpretation.**

*Keywords:* stars: coroneae — stars: neutron — X-rays: individual (MXB 1730–335) — X-rays: binaries — X-rays: bursts

### 1. INTRODUCTION

The Rapid Burster (hereafter RB), also named MXB 1730–335, is a transient low mass X-ray binary (LMXB), with outbursts lasting for a month and recurring every 7 months (Masetti 2002). The RB was discovered in 1976 by Lewin et al. (1976), located in globular cluster Liller 1, at a distance 7.9 kpc (Valenti, Ferraro & Origlia 2010), with the most salient feature of type-II X-ray bursts in quick succession with short intervals 10 s during certain periods. For distinguishing it from the nearby type-I X-ray burster, which produces type-I X-ray bursts with long intervals  $\sim$  ks, it was named the Rapid Burster. Type-I X-ray bursts, also named thermonuclear bursts, are caused by unstable burning of the accreted hydrogen/helium supplied by the low-mass companion star (for reviews, see Lewin, Van Paradijs & Taam 1993; Cumming 2004; Strohmayer & Bildsten 2006; Galloway et al. 2008). Correspondingly, the nearby (only 0.°5 from the RB) bright type-I X-ray burster 4U 1728–34 was named the Slow Burster (hereafter the SB), which is generally difficult for non-imaging telescopes to distinguish between the two bursters.

The Rapid Burster also produces type I bursts during its outbursts, with a recurrent timescales of hours (Hoffman, Marshall & Lewin 1978). Different from the RB, the bursting pulsar (hereafter BP, also named GRO J1744–228) (Fishman et al. 1995), with both pulsations (a period of 467 ms) (Kouveliotou et al. 1996) and type-II bursts detected, shows no type-I bursts. Type I bursts in the RB occur in outburst from 45 percent of the Eddington luminosity to almost quiescence (Bagnoli et al. 2013). However, type II bursts only appear below a critical luminosity of about 10 percent the Eddington luminosity (Guerrero et al. 1999). The behavior of the type II bursts from the RB exhibits a series of burst patterns. It is believed that three modes (Marshall et al. 1979; Guerrero et al. 1999) follow one another in a smooth transition to phenomenologically describe type II bursting behaviour, i.e., mode 0, mode 1 and mode 2, with duration and complexity behavior decreasing gradually. Based on population study of the type II bursts from the RB, rather than the mode 0–2, Bagnoli et al. (2015) prefer adopting a simple classification between long and short bursts, which reflects whether they interact with the persistent emission.

Type-II X-ray bursts vary in duration from 130 ms to 11 min and interval from seconds to an hour (Bagnoli et al. 2015), with peak luminosities up to the Eddington luminosity  $L_{\text{Edd}}$ . In contrast to thermonuclear flashes on a NS surface causing type-I bursts, the type-II bursts are attributed instead to episodic accretion instabilities (Lewin, Van Paradijs & Taam 1993). The most important and unique property of the RB is that the type-II bursts have a relaxation-oscillator behaviour: a clear correlation between the burst fluence,  $E$  and the waiting time to the next burst,  $\Delta t$  (known as  $E - \Delta t$  relation) (Lewin et al. 1976). Naturally, an explanation to the relaxation-oscillator behaviour is that a reservoir of accretion mass is accumulated around the neutron star (Lewin, Van Paradijs & Taam 1993). The mass from the reservoir releases the gravitational energy during the burst, and the reservoir will be refilled until the next burst. However, the mechanisms of type II bursts remain largely a puzzle in how the accretion material releases its potential energy in the innermost disk or near the NS surface. Basically there is a dichotomy between magnetospheric and nonmagnetospheric models for the generation of the type II bursts from the RB, characterized by magnetospheric instability and disk instability, respectively (for reviews, see Lewin, Van Paradijs & Taam 1993; Spruit&Taam 1993; Lewin, Van Paradijs & Taam 1995; Bagnoli et al. 2015).

The RB was observed by Hard X-ray Modulation Telescope (HXMT) with a total exposure time of 60 ks in August 2017. Accompanied with simultaneous Swift/XRT data, the large effective area and broad band energy provide us an excellent opportunity to explore the burst behaviour of the RB. This paper is organized as follows: We present the Insight-HXMT and Swift/XRT observations used in this work of the RB and describe the data reduction procedures in Section 2. The next section (Section 3) describes the HXD detection and the burst spectral evolution, by stacking dozens bursts. We give the possible understandings upon the observed phenomena in the last section (Section 4).

## 2. OBSERVATIONS AND DATA ANALYSIS

To explore the source state of the RB in Insight-HXMT observations, we take the Swift/BAT light curves. As shown in Fig. 1, the upper limit of the flux is  $15 \text{ mCrab}^1$ , suggesting that the **bursts** are located at the end of the outburst and evolves toward the quiescent state.

We use XSPEC v12.10.0 for the spectral analysis. **The interstellar absorption model takes a column density fixed at  $3.64 \times 10^{22} \text{ atoms/cm}^2$  (van den Eijnden et al. 2017), which is derived from a model consisting of a multicolor disk model (diskbb in XSPEC Mitsuda et al. 1984) and a disk reflection emission by fitting the persistent emission of the RB.** The parameters of the X-ray spectra fitting model are estimated with 68% ( $1 \sigma$ ) confidence level.

### 2.1. *Insight-HXMT*

HXMT (also dubbed as Insight-HXMT, Zhang et al. 2014, Zhang et al. 2020) excels in a broad energy band (1–250 keV) and a large effective area in hard X-rays energy band. It consists of three slat-collimated instruments: the High Energy X-ray Telescope (HE, with a collection area  $5103 \text{ cm}^2$ , 20–250 keV)(Liu et al. 2020), the Medium Energy X-ray Telescope (ME, with a collection area  $952 \text{ cm}^2$ , 5–30 keV)(Cao et al. 2020), and the Low Energy X-ray Telescope (LE, with a collection area  $384 \text{ cm}^2$ , 1–10 keV)(Chen et al. 2020).

HEASOFT version 6.22.1 and Insight-HXMT Data Analysis software (HXMTDAS) v2.01 are used to analyze the data. Only the small field of view (FoV) mode of LE and ME is used, for preventing the contaminations from near-

<sup>1</sup> <https://swift.gsfc.nasa.gov/results/transients/>

by sources and the bright earth. The good time interval is filtered with the recommended criteria in HXMT Data Reduction Guide Version 2.01 given by the Insight-HXMT team.

Among the outburst of the Rapid Burster (RB) in 2017, there are 7 obsids on the Slow Burster (SB), covering the time span between August 26th and 28th. Due to the large FoV of Insight-HXMT, the RB was also detected in the FoV of these observations. We performed a visual inspection of the light curves of the obsids, which results in totally  $\sim 200$  bursts, including a type-I X-ray burst. All the type II bursts have a similar profile, seconds duration and tens seconds **recurrence** time, indicating that all of them are during mode-2 bursting phases towards the end of the outburst.

LE and ME each contains 3 independent detector boxes, each with elongated rectangle FoV and different orientations. In these observations, the SB is located at the center of the FoVs and the RB is off center. If the bursts are from the SB, the fluxes of the 3 boxes should be roughly same, otherwise from RB. The average flux of the type-I X-ray burst by the three LE boxes in 1–10 keV is  $68.0 \pm 1.5$ ,  $70.5 \pm 1.6$  and  $68.2 \pm 1.5$ , respectively. The roughly same counts rates in three boxes of LE or ME denote that the type-I burst should originate from the SB.

From these type-II X-ray bursts, we choose 159 bursts to analyse, which satisfies the good-time-interval selection criteria of LE and ME simultaneously, as shown in Table 1. Among them, the bursts of the first three obsids have longer time intervals 150–280 s. For the last three obsids, the bursts have shorter time intervals 30–50 s. For the bursts in the 4th obsid, both of the interval and duration vary significantly. Additionally, there is a type-I X-ray burst in this obsid. Based on the main characteristics of the bursts, we divide the bursts into two groups to analysis: the long bursts in the first 3 obsids (TOO1) and the short burst in the last 3 obsids (TOO2).

In the light curve and spectral analysis, we use the time when the burst reached its peak of ME as a reference for producing the light curve and spectrum of the each burst. With respect to the reference time, for the bursts of TOO1 and TOO2, we split each burst into a sequence of 1 s slices after the burst onset, and stack the light curve slices in chronological order. For the burst spectra of TOO1 and TOO2, we split each burst into a sequence of 2 s and 1 s slices after the burst onset, respectively. Because of high background and low flux of the RB detected by HE, only the LE and ME data are used to explore the evolution of the bursts. We use the ftool *addspec* to stack the spectral slices in chronological order, and fit the time-ordered stacked spectra.

Those time periods without burst are adopted as background, which includes instrumental background, cosmic diffuse background and persistent/non-burst flux of the RB and the SB, for investigating the burst spectrum evolution.

## 2.2. *Swift/XRT*

Within the same day when Insight-HXMT detected bursts from the RB, Swift/XRT also observed the source. The XRT observation was performed **2.8** hours after the Insight-HXMT observations, and cover a period of MJD 57991.69025 (UTC 2017-08-26 16:32:48)–57991.95835 (UTC 2017-08-26 22:58:56). The OBSID is 00031360136 with an exposure 2 ks. The standard data process procedure of the timing mode is carried out using the ftools package with standard procedures (xrtpipeline version 0.13.5)<sup>2</sup>. To avoid spectral pile-up distortions, the spectra of source and background are extracted from a source region and a source-free background region with the grade 0.

A first inspection of the light curves shows strong variability with several bursts, and the maximum count rate is 110 cts/s. From the shapes of the bursts, as shown in Fig. 3, totally, 12 type-II bursts and 1 type-I burst are detected by Swift/XRT. The persistent/non-burst emission is stable in this observation, remaining at a count rate 2 cts/s.

## 3. RESULTS

### 3.1. *Persistent emission*

We fit the persistent spectrum observed by Swift/XRT, as show in Fig. 4, with a model consisting of an interstellar absorption TBabs (Wilms et al. 2000), a power law and a diskbb. We find an acceptable fit:  $\chi^2_{\nu} = 0.83$  ( $\nu$  17; Fig. 4). The unabsorbed bolometric flux in 1–10 keV is  $4.9^{+0.6}_{-1.2} \times 10^{-10}$  erg cm<sup>-2</sup> s<sup>-1</sup>, corresponding to a **luminosity** of  $3.6 \pm 0.4 \times 10^{36}$  erg s<sup>-1</sup> at a distance of 7.9 kpc.

We explore a number of different fits, e.g., TBabs\*(bbody+powerlaw), and find that the blackbody model yields a good fit, with similar temperature, photo index and  $\chi^2_{\nu}$  as derived from the diskbb model. The energy range of the spectrum prevents us adopting more complex components to replace the power law model, e.g., a cutoff-powerlaw or a disk-reflection model.

<sup>2</sup> <https://swift.gsfc.nasa.gov/analysis/>

### 3.2. Timing properties

Since low count rate of LE&ME makes difficult to analyze individual burst, we adopt a method that stacking bursts light curves and spectra. For TOO1 and TOO2, the lightcurves of 23 and 117 bursts are stacked respectively. As shown in Fig. 2, the stacked light curves of the bursts from the two groups have a similar trends in rise and decay, in the energy range 1–10 and 10–20 keV, respectively. The profile of the burst of TOO1 and TOO2 is a Gaussian-like profile with a similar rising and decay time. However, different from TOO2, the peak of LE and ME in TOO1 occurs not simultaneously, i.e., there is a 3 s delay of hard X-ray emission with respect to the soft X-ray emission. For the sake of clarity, the soft X-ray flux and the hard X-ray flux are scaled into a same panel. However, the low count rate and short burst duration prevent us from re-bining the lightcurve of the TOO2 bursts with smaller time bin. As shown in Fig. 2, the burst width is roughly same in the soft and hard X-ray band.

### 3.3. Broad band spectrum

The first attempt to model the spectrum during the burst evolution is an absorbed blackbody. However, the result of the  $\chi^2_\nu$  (with  $\nu$  43–83) are mostly larger than 2, whether let the  $N_{\text{H}}$  free or not during spectral fitting.

An alternative model for the type-II X-ray burst is an absorbed Comptonization model (comptt in XSPEC) (Titarchuk 1994). This model yields a reasonable fit with  $\chi^2_\nu \sim 1$  (with  $\nu$  43–83). First, we let the seed photon energy  $T_{\text{seed}}$  and optical depth  $\tau$  free during fitting. In the course of the burst evolution, the fit results indicate the  $T_{\text{seed}}$  always around 0.2 keV, both for TOO1 and TOO2;  $\tau$  is 8.7 and 10 for TOO1 and TOO2, respectively. Hence, we fixed  $T_{\text{seed}}$  and  $\tau$  to explore the burst evolution, resulting variations are qualitatively very similar to those measured with the free values, as shown in Fig. 4.

The improved spectral fitting results in the electron temperature  $kT_e$  2–3 keV and the reduced  $\chi^2_\nu$  0.7–1.4 with the  $\nu$  43–83. As shown in Fig. 5, both for TOO1 and TOO2, the profile of  $N_{\text{comptt}}$  is similar, peaking at the center of the burst. A similar trend is also found for  $kT_e$  in TOO2. For TOO1 with the HXD phenomenon,  $kT_e$  shows a substantial increase from 2 to 3 keV. We combine the tail of the burst spectra and find that  $kT_e$  returns to 2 keV as measured at the initial phase.

The burst unabsorbed bolometric peak fluxes in 1–30 keV of TOO1 and TOO2 are obtained as  $12.3 \pm 0.3$  and  $7.0 \pm 0.1 \times 10^{-9}$  erg cm $^{-2}$  s $^{-1}$ , corresponding to  $9.2 \pm 0.2$  and  $5.2 \pm 0.1 \times 10^{37}$  erg s $^{-1}$  at a distance of 7.9 kpc, respectively.

**We notice that** the spectral evolution of the heartbeat mode variability in GRS 1915+105 is well described by a diskbb model in the course of the burst (Taam et al. 1997; Paul et al. 1998), with the disk  $kT$  changed from 1.1 to 2 keV (Mineo et al. 2012). We analysed the burst spectra of the RB with the same model, and yield an acceptable reduced  $\chi^2$ . However, the disk  $kT$  is up to 3 keV, which is too high for a NS X-ray binary.

## 4. DISCUSSION AND SUMMARY

We have analyzed the decay phase of the outburst experienced by the RB during 2017 observed by Insight-HXMT in a broad energy band. By stacking the type-II bursts with recurrence time of 100–300 seconds, we find for the first time a time delay of about 3 seconds at hard X-rays. The energy spectrum of the burst can be denoted by a Comptonization model, for which the temperature of the seed photons, the optical depth, the temperature of the hot plasma are derived with values of 0.2 keV, 9–10 and 2–3 keV, respectively. These findings put more constraints upon the models at work for the RB.

The tight relation between the burst strength and the waiting time (Lewin et al. 1976) leads to a series of models in history proposed via focusing on the sudden release of the accretion power in the disk. Type-II burst can be caused by the instability of the disk on viscous (Lightman & Eardley 1974) or thermal time scales (Shakura & Sunyaev 1976), the magnetic barrier (D’Angelo & Spruit 2010, 2012) or the magnetic reconnection on the disk (Jiang Stone & Davis ).

However, all models have their own shortages in covering all the features observed in the RB (Lewin, Van Paradijs & Taam 1993). The possible breakthrough to discriminate different models may come from the joint observations carried out in 2015 by XMM, Swift/XRT and Nustar (van den Eijnden et al. 2017). With this campaign, both the continuous and the mode-0 burst spectra were well measured in a rather broad energy band of 1–30 keV. It turns out that, the inner radius keeps staying at round  $41 R_g$  ( $R_g = 2GM/c^2$ ) for both burst and pre-burst emissions, and the corona temperature of the pre-burst is 7.19 keV, which is significantly larger than 2.42 keV measured for the

non-thermal temperature of the burst. Comparison for the corona temperatures between burst and pre-burst are always challenged by the contamination source 4U 1728–34 which is located only  $0.^\circ 5$  away from the RB. We note that less change of the burst temperature with respect to the pre-burst was reported in ASCA (Mahasena et al. 2003) and BeppoSAX (Masetti et al. 2000), which is probably due to limited bandwidth (i.e. below 10 keV) of the former and the relatively poorer statistics of the latter which does not allow to well constrain the parameters in *comptt* model. If the burst is caused by the temporary accretion on the disk, via either disk instability or the magnetic barrier, the inner disk radius should evolve to be smaller than that of the pre-burst. Regarding to the temperature difference of the corona between burst and pre-burst, the hot corona wherever is located, either in boundary layer or around the disk, can in principle be cooled by the seed photons of the burst shower. However, in history there are no hints for detecting such a cooling procedure in phase-resolved burst spectrum and all showed a constant corona temperature around 2 keV as derived from observations of ASCA (Mahasena et al. 2003) and RXTE (Bagnoli et al. 2015). Here Insight-HXMT provides an additional clue for supporting no cooling effect for the corona during the burst. These results hence support a temporary show-up of an additional corona with temperature around 2 keV, via a mechanism of e.g. magnetic reconnection on the disk but rather than instability of the disk accretion.

During the decay phase of the 2017 outburst, Insight-HXMT observed for the type-II burst that the flux in 10–20 keV lags 3 seconds than that in 1–10 keV. Time delay of a few seconds was also reported in the heart-beat mode of micro-quasar GRS 1915+105 (Janiuk & Czerny 2005; Neilsen et al. 2011; Massa et al. 2013). Bagnoli et al. (2015) found in the RB the heart beat oscillation similar to GRS 1915+105 from RXTE observations. However, a further investigation by Maselli et al. (2018) revealed no time lag between soft and hard X-rays during the two RXTE observations where the heart beat of the RB was discovered. Modellings of such hard X-ray delay are relatively rare so far and among a few trials are those from Janiuk & Czerny (2005); Neilsen et al. (2011); Massa et al. (2013). Janiuk & Czerny (2005) considered radiation-pressure instability (Lightman & Eardley 1974) in the inner disk parts and showed that the hard X-ray delays can be caused by the time needed for the corona to adjust to the changing conditions in the underlying disk. In their theory, due to the instability of the radiation pressure mass of the inner accretion flow can be exchanged between the disk and the corona via heating and evaporation, which forms a “density wave” around  $20\text{--}30 R_g$  to cause a loop. Accordingly, the density of the corona evolves with time, which can end up at time scale of 1 second. Here we render the similar scenario for the hard X-ray time lag observed in type-II burst of the RB. We consider an instability caused by magnetic reconnection on the disk. Such a magnetosphere storm resulted from disk magnetic reconnection was initially proposed by Davidson (1982). Magnetic reconnection can supply power to heat the disk and hence play a role in producing a temporary corona on top of the disk via extracting the accretion materials from the disk. Such a corona formation procedure can in principle result in hard X-ray delay at time scale of second in a way induced in Janiuk & Czerny (2005). Regarding to the corona temperature, Zhang et al. (2000) showed that, the magnetic reconnection in the disk can produce a so-called warm layer, i.e. a corona with low temperature covering the cold disk, as shown in Fig. 6. Therefore, we speculate that the temporary warm layer born out of the disk magnetic reconnection may correspond to the type-II burst observed in rapid burster.

In Zhang et al. (2000) the warm layer is supposed to be optical thick, which is consistent with the optical depth as measured during the type-II burst. We calculate the flux of the disk (*diskbb*) and warm layer (*comptt*) in units of  $\text{photon cm}^{-2} \text{s}^{-1}$  with those model parameters derived in broad band spectral fitting with Insight-HXMT, and find that the two values are roughly same. This calculation indicates that nearly all of the disk emission are scattered to higher energy by the warm layer, and hence fits the scenario that part of disk is fully covered by the temporarily produced corona. We notice that in Fig. 5 the corona temperature keeps increasing for long burst in TOO1 but turns over for short burst in TOO2. If the corona temperature is assumed to be the virial temperature (Janiuk & Czerny 2005), then during burst the temporary corona moves inward would lead to an increase in temperature. For the short burst in TOO2, gradual cease of the power supply from the disk magnetic reconnection in the decay phase of the burst can induce a drop in corona temperature.



**In summary, the broad band observations of the rapid burster by Insight-HXMT reveal several interesting temporal and spectral properties of the type-II bursts born out of the outburst decay in 2017. These findings may be accounted for via introducing a temporary warm layer produced with disk magnetic reconnection. Further investigations upon the RB observed and the bursting pulsar by Insight-HXMT can definitely provide more clues to pin down this puzzle.**

#### ACKNOWLEDGMENTS

This work made use of data from the Insight-HXMT mission, a project funded by China National Space Administration (CNSA) and the Chinese Academy of Sciences (CAS). This work is supported by the National Key R&D Program of China (2016YFA0400800) and the National Natural Science Foundation of China under grants U1838201, U1938101, U1838202, 11473027, 11733009, U1838115.

#### REFERENCES

- Bagnoli, T., & in't Zand, J. J. M. 2015, *MNRAS*, 450, L52
- Bagnoli, T., in't Zand, J. J. M., Galloway, D. K., Watts A. L., 2013, *MNRAS*, 431, 1947
- Bagnoli, T., in't Zand, J. J. M., D'Angelo, C. R., Galloway, D. K., 2015, *MNRAS*, 449, 268
- Cao, X. L., Jiang, W. C., Meng, B., et al. (Insight-HXMT team), 2020, *Sci. China-Phys. Mech. Astron.*, 63, 249504
- Chen, Y., Cui, W. W., Li, W., et al. (Insight-HXMT team), 2020, *Sci. China-Phys. Mech. Astron.*, 63, 249505
- Cumming, A. 2004, *Nucl. Phys. B Proc. Suppl.*, 132, 435
- D'Angelo C. R., Spruit H. C., 2010, *MNRAS*, 406, 1208
- D'Angelo C. R., Spruit H. C., 2012, *MNRAS*, 420, 416
- Davidson, G. T., 1982, *ApJ*, 255, 705
- Fishman, G. J., Kouveliotou, C., van Paradijs, J., Harmon, B. A., Paciesas, W. S., Briggs, M. S., Kommers, J. M., & Lewin, W. H. G. 1995, *IAU Circ.*, No. 6272
- Galloway, D. K., Munro, M. P., Hartman, J. M., et al. 2008, *ApJS*, 179, 360
- Guerrero, R., Fox, D. W., Kommers, J., et al., 1999, *MNRAS*, 307, 179
- Hoffman, J. A., Marshall, H. L., & Lewin, W. H. G., 1978, *Nature*, 271, 630
- Janiuk, A. & Czerny, B. 2005, *MNRAS*, 356, 205
- Jiang Y.-F., Stone J. M., Davis S. W., 2014, *ApJ*, 784, 169
- Kouveliotou, C., van Paradijs, J., Fishman, G. J., Briggs M. S., Kommers, J., Harmon, B. A., Meegan C. A., Lewin W. H. G., 1996, *Nature*, 379, 799
- Lewin, W. H. G., Doty, J., Clark, G. W., et al., 1976, *ApJ*, 207, L95
- Lewin, W. H. G., van Paradijs, J., & Taam, R. E., 1993, *Space Sci. Rev.*, 62, 223
- Lewin, W. H. G., van Paradijs, J., & Taam, R. E., 1995, in *X-Ray Binaries*, ed. W. H. G. Lewin, J. van Paradijs, & E. P. J. van den Heuvel (Cambridge: Cambridge Univ. Press), 175
- Lightman A. P., Eardley D. M., 1974, *ApJ*, 187, L1
- Liu, C. Z., Zhang, Y. F., Li, X. F., et al. (Insight-HXMT team), 2020, *Sci. China-Phys. Mech. Astron.*, 63, 249503
- Mahasena P., Inoue H., Asai K., Dotani T., 2003, *PASJ*, 55, 827
- Marshall, H. L., Hoffman, J. A., Doty, J., Lewin, W. H. G., Ulmer, M. P., 1979, *ApJ*, 227, 555
- Maselli A., Capitanio F., Feroci M. et al., 2018, *A&A*, 612, 33
- Masetti N., 2002, *A&A*, 381, L45
- Masetti, N., Frontera, F., Stella, L. et al., 2000, *A&A*, 363, 188
- Massa, F., Massaro, E., Mineo, T., et al., 2013, *A&A*, 556, A84
- Mineo, T., Massaro, E., D'Ai, A., et al. 2012, *A&A*, 537, A18
- Mitsuda, K., Inoue, H., Koyama, K., et al. 1984, *PASJ*, 36, 741
- Neilsen, J., Remillard, R. A., & Lee, J. C. 2011, *ApJ*, 737, 69
- Paul, B., Agrawal, P. C., Rao, A. R., et al. 1998, *ApJ*, 492, L63
- Shakura N. I. & Sunyaev R. A., 1976, *MNRAS*, 175, 613
- Spruit, H. C., Taam, R. E., 1993, *ApJ*, 402, 593
- Strohmayer, T., & Bildsten, L. 2006, *New views of thermonuclear bursts (Compact stellar X-ray sources)*, 113, 156
- Taam, R. E., Chen, X., & Swank, J. H. 1997, *ApJ*, 485, L83
- Titarchuk, L., 1994, *ApJ*, 434, 313
- Valenti, E., Ferraro, F. R., Origlia, L., 2010, *MNRAS*, 402, 1729
- van den Eijnden, J., Bagnoli, T., Degenaar, N., Lohfink, A. M., Parker, M. L., in't Zand, J. J. M., Fabian, A. C., 2017, *MNRAS*, 466, L98
- Wilms, J., Allen, A., & McCray, R. 2000, *ApJ*, 542, 914

Zhang, S. N., et al., 2000, *Science*, 287, 1239

Zhang, S., Lu, F. J., Zhang, S. N. et al., in *Space Telescopes and Instrumentation 2014: Ultraviolet to Gamma Ray*, Proc. SPIE, Vol. 9144 (2014) p. 914421

Zhang, S. N., Li, T. P., Lu, F. J., et al. (Insight-HXMT team), 2020, *Sci. China-Phys. Mech. Astron.*, 63, 249502

**Table 1.** The type-II X-ray bursts detected by Insight-HXMT during 2017 outburst from the RB.

| OBSID                        | Start Time          | Elapsed Time (s) | GTI (s) | $n_{\text{burst}}$ | $t_{\text{averageinterval}}(\text{s})$ |
|------------------------------|---------------------|------------------|---------|--------------------|--|
| P010130300101-20170826-01-01 | 2017-08-26T13:45:21 | 11760            | 1980    | 7                  | 282.9                                  |
| P010130300102-20170826-01-01 | 2017-08-26T17:16:56 | 6600             | 1635    | 9                  | 181.7                                  |
| P010130300103-20170826-01-01 | 2017-08-26T20:27:50 | 5820             | 1136    | 7                  | 162.3                                  |
| P010130300104-20170826-01-01 | 2017-08-26T23:38:44 | 11880            | 1718    | 19                 | 90.4                                   |
| P010130300201-20170828-01-01 | 2017-08-28T16:43:29 | 6120             | 1620    | 31                 | 52.3                                   |
| P010130300202-20170828-01-01 | 2017-08-28T20:11:30 | 5880             | 1086    | 31                 | 35.0                                   |
| P010130300203-20170828-01-01 | 2017-08-28T23:22:25 | 12120            | 1785    | 55                 | 32.5                                   |

**Table 2.** The spectral fit results of the persistent emission by Swift/XRT.

| $T_{\text{in}}$ (keV)  | $R_{\text{in}}^{*a}$ ( $10^2\text{km}$ ) | $\Gamma$               | $N^{*b}$               | $\chi^2_{\nu}$ |
|------------------------|--|------------------------|------------------------|----------------|
| $0.21^{+0.16}_{-0.09}$ | $1.65^{+149}_{-0.81}$                    | $1.97^{+0.18}_{-0.15}$ | $9.57^{+2.29}_{-3.48}$ | 0.83(17)       |

a : the inner radius of the disk with a distance of 7.9 kpc and an inclination angle of  $29^\circ$ .

b : in unit of  $10^{-2}$  photons/keV/cm<sup>2</sup>/s at 1 keV.



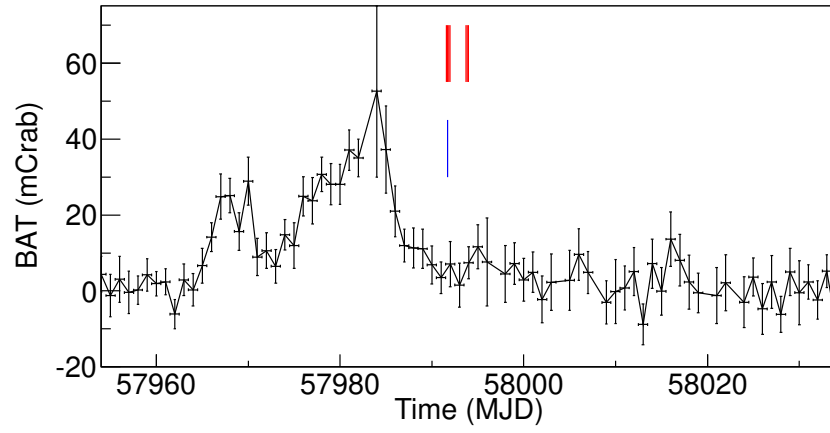


**Figure 1.** Daily lightcurves of the Rapid Burster by Swift/BAT during the outbursts in 2017 in 15–50 keV. The observations of Insight-HXMT and Swift/XRT are indicated by vertical lines by red and blue respectively.

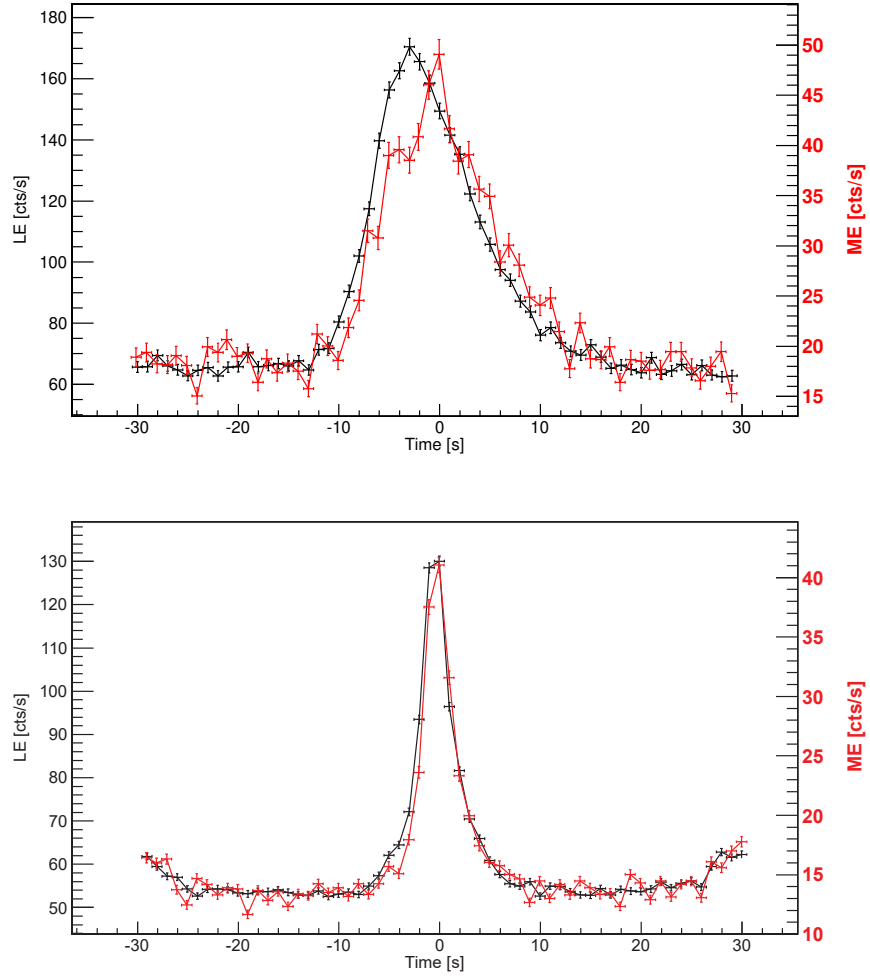


**Figure 2.** The stacked Insight-HXMT/LE and Insight-HXMT/ME light curves of the RB at 1–10 keV and 10–20 keV for TOO1 (the top panel) and TOO2 (the below panel). We note that in the upper panel, the hard X-ray emission (red) lags the soft ones, i.e., the HXD phenomenon.

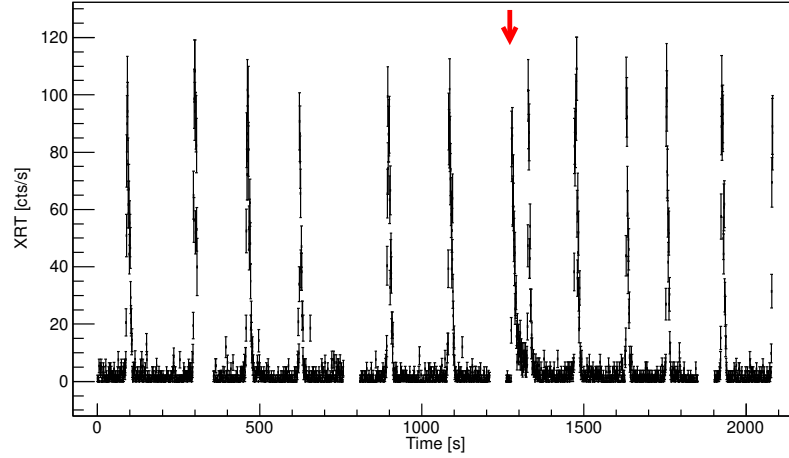


**Figure 3.** Sandwiched light curve of the RB during its 2017 outburst observed by Swift/XRT, for the complete Swift/XRT bandpass at 1 s resolution. Data gaps (50 s) mark jumps in time when there were no GTIs. The red arrow indicates a type I X-ray burst from the RB.

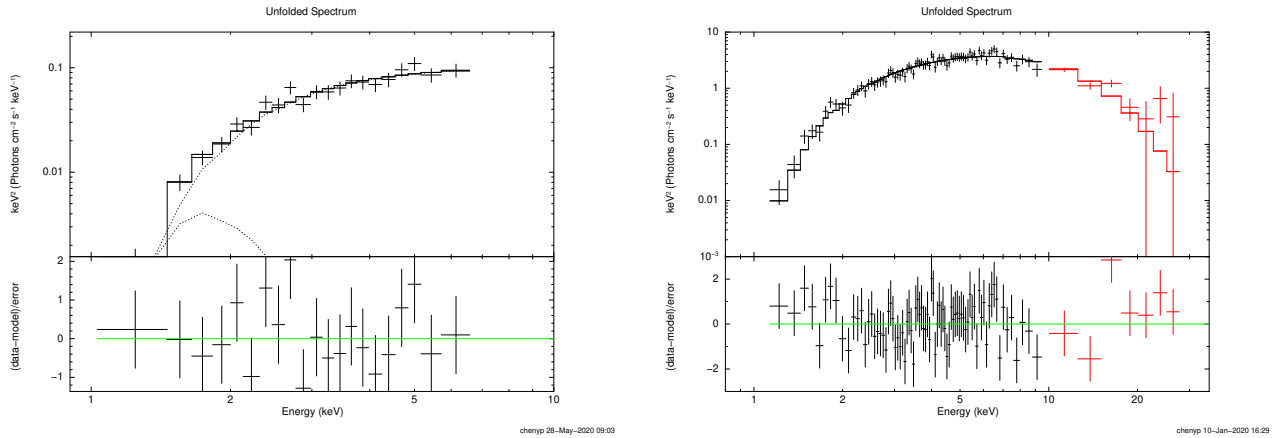


**Figure 4.** The unfolded spectra of the persistent/non-burst emission detected by Swift/XRT and the spectra of the TOO1 burst at the peak flux observed by HXMT/LE (black) and HXMT/ME (red) are given in left and right panel respectively.

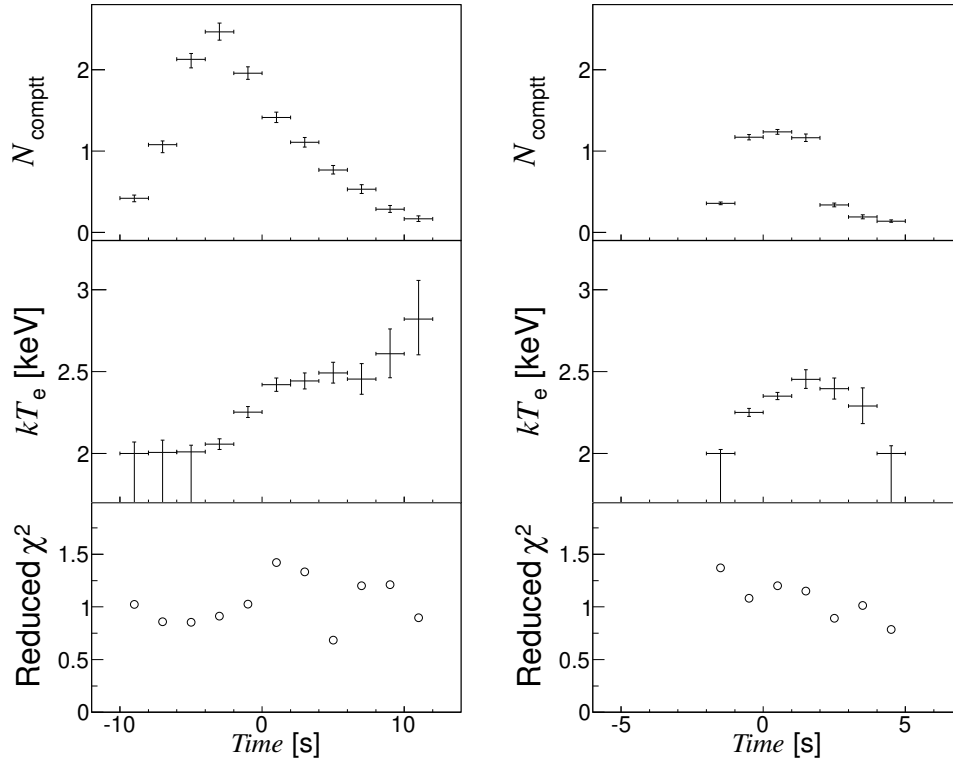


**Figure 5.** Time-resolved spectroscopy of the X-ray bursts using an absorbed compTT model for the TOO1 (the left panel) and TOO2 (the right panel), in time bin 2 s and 1 s respectively. The normalization  $N_{\text{comp}}$ , the electron temperature  $kT_e$  and the reduced  $\chi^2$  statistic are given in the top, middle and bottom panels respectively.

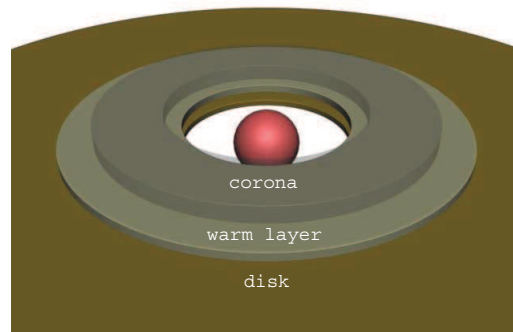


**Figure 6.** Illustration of the central region of an NS XRB during a type-II X-ray burst, in which the warm layer locates above the disk.

